This is an open access article published under an ACS AuthorChoice License, which permits copying and redistribution of the article or any adaptations for non-commercial purposes.

Journal of Medicinal Chemistry

pubs.acs.org/jmc Article

A Multipronged Approach Establishes Covalent Modification of β-Tubulin as the Mode of Action of Benzamide Anti-cancer Toxins

Juan Manuel Povedano,[▽] Rameshu Rallabandi,[▽] Xin Bai, Xuecheng Ye, Joel Liou, Hong Chen, Jiwoong Kim, Yang Xie, Bruce Posner, Luke Rice, Jef K. De Brabander,* and David G. McFadden*

Cite This: J. Med. Chem. 2020, 63, 14054−14066 Read Online

ACCESS | Metrics & More | Article Recommendations | Supporting Information

ABSTRACT: A phenotypic high-throughput screen identified a benzamide small molecule with activity against small cell lung cancer cells. A "clickable" benzamide probe was designed that irreversibly bound a single 50 kDa cellular protein, identified by mass spectrometry as β-tubulin. Moreover, the anti-cancer potency of a series of benzamide analogs strongly correlated with probe competition, indicating that β-tubulin was the functional target. Additional evidence suggested that benzamides covalently modified Cys239 within the colchicine binding site. Consistent with this mechanism, benzamides impaired growth of microtubules formed with β-tubulin harboring Cys239, but not β_3 tubulin encoding Ser239. We therefore designed an aldehyde-containing analog capable of trapping Ser239 in β_3 tubulin, presumably as a hemiacetal. Using a forward genetics strategy, we identified benzamide-resistant cell lines harboring a Thr238Ala mutation in β-tubulin sufficient to induce compound resistance. The disclosed chemical probes are useful to identify other colchicine site binders, a frequent target of structurally diverse small molecules.

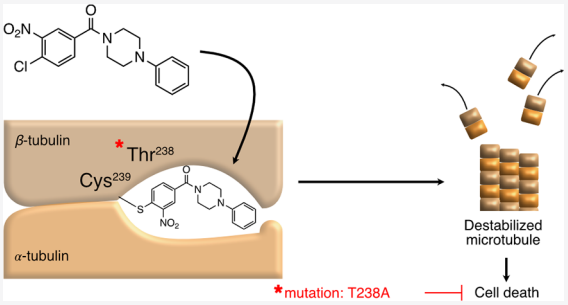

INTRODUCTION

The identification and development of new cancer therapies remain a challenge. Target-based screens have proven effective at identifying small molecule inhibitors for oncogenic kinases that are recurrently mutated in many cancers. However, for tumors without mutations in these kinases, phenotypic screens offer a powerful complementary approach in which small molecules with anti-cancer activity can be identified in high-throughput format. The establishment of preliminary structure−activity relationships around these initial HTS hits is essential to facilitate the development of chemical probes suitable for target identification. If the biological target lends itself to a more translational evaluation, then more sophisticated medicinal chemistry optimization is useful for initial in vivo proof of concept studies in animal models of human cancer.

Small cell lung cancer (SCLC) is an aggressive neuroendocrine (NE) malignancy, and a diagnosis of SCLC portends poor survival. Treatments for SCLC have remained largely unchanged, and cytotoxic chemotherapies remain the foundation of therapy for SCLC. The failure to improve outcomes in SCLC stems in part from a lack of recurrent mutations that encode chemically tractable proteins. We leveraged genetically defined cancer cell lines derived from a mouse model of SCLC to facilitate phenotypic screening for anti-cancer small molecules with activity against SCLC and other NE tumors.[1−4] Here, we report the identification of a series of benzamides that exhibit anti-cancer activity to murine and human SCLC cell lines. We utilize a combination of medicinal chemistry, probe reagent development, forward genetics, and *in vitro* assays of microtubule dynamics to demonstrate that these small molecules covalently modify β-tubulin via nucleophilic aromatic substitution.

RESULTS AND DISCUSSION

Identification and Structure−Activity Relationship Studies (SAR) of Benzamide SCLC Toxins. We identified a benzamide-phenyl piperazine from a phenotypic high-throughput chemical screen aimed at identifying small molecules with selective anti-cancer activity against a panel of mouse and human SCLC cell lines. Benzamide **1** was active against three independent murine SCLC (mSCLC) cell lines with an average EC_{50} of 3.21 ± 0.6 μM (Figure 1A,B). Moreover, three human SCLC cell lines, H889, H2107, and H128, exhibited sensitivity, suggesting conserved expression of the protein target of compound **1** in mouse and human cells (Supporting Information Figure 1). A literature search identified a previous study reporting that benzamide **1** was toxic to yeast cells through inhibition of Sec14, a protein

Received: September 11, 2020
Published: November 12, 2020

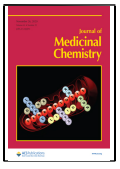

ACS Publications © 2020 American Chemical Society

A

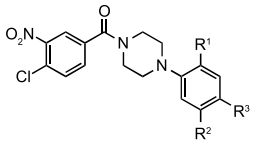

cpd	R^1	R^2	R^3	IC_{50} (nM)
1	H	H	H	4,358 (±1,010)
2	Cl	H	H	2,947 (±203)
3	H	OCH_3	H	1,562 (±248)
4	H	CH_3	H	1,420 (±174)
5	CH_3	CH_3	H	1,042 (±102)
6	H	Br	H	866 (±61)
7	H	Cl	H	694 (±38)
8	H	CN	H	593 (±109)
9	Cl	Cl	H	458 (±66)
10	CH_3	Cl	H	182 (±31)
11	H	H	F	21,050 (±2,680)
12	F	H	H	7,939 (±815)
13	F	H	F	24,690 (±2,910)
14	CH_3	H	CH_3	6,986 (±747)
15	H	H	OCH_3	40,330 (±11,500)

B

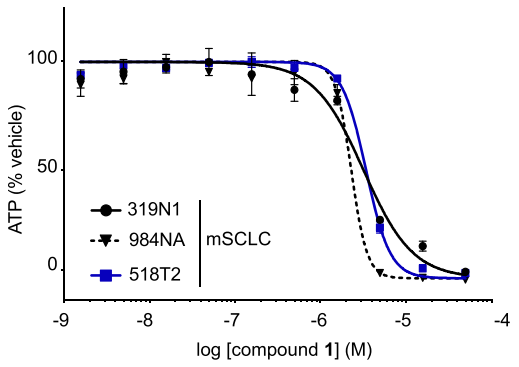

C

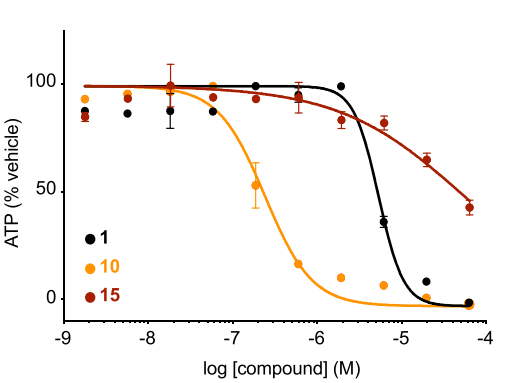

Figure 1. Structure−activity relationships of 4-chloro-3-nitrobenzamide SCLC toxins. (A) Table with half-maximal inhibitory concentrations (IC_{50}) for benzamide analogs **1**−**15** against murine SCLC cell line 319N1. Standard error is indicated between brackets and is based on $n = 2$ technical replicates. (B) Dose−response curves of compound **1** against three murine SCLC cell lines. (C) Dose−response curves of compounds **1**, **10**, and **15** against murine SCLC cell line 319N1.

essential for membrane trafficking in the Golgi-endosomal system.[5] However, less than 30% amino acid sequence conservation between yeast and mammalian Sec14 orthologs raised the possibility that compound **1** induced SCLC cell death through Sec14-independent mechanisms. We therefore initiated an unbiased medicinal chemistry and forward genetics approach to identify the target of benzamide **1**.

We synthesized analogs of compound **1** to understand structure−activity relationships that would enable the development of chemical probes for target identification. Systematic modification to the phenyl piperazine ring revealed that substitutions at the R^1, R^2, and R^3 positions impacted toxicity (Figure 1A,C). The chlorine substituent at position R^1 slightly improved potency (**2**), whereas *ortho*-fluorine analog **12** was 2-fold less active than parent benzamide **1**. At the R^2 position, bromine, chlorine, and cyano groups improved activity ∼5 to 7-fold (analogs **6**−**8**), whereas *meta*-methyl and methoxy-substituted analogs **3** and **4** were only ∼3-fold more potent. Of the various 2,5-disubstituted combinations tested, analog **10** (R^1 = Me and R^2 = Cl) was the most potent benzamide with an EC_{50} of 182 nM. In contrast, modifications at the *para*-position (R^3 = F, Me, and MeO; analogs **11** and **13**−**15**) significantly impacted the cytotoxic activity within this series.

Initial experiments had shown that the 4-chloro-3-nitro substitution pattern was an essential feature required for the ability of the benzamides to affect growth of the mSCLC cell line 319N1. For example, removing either of these substituents from the benzamide ring resulted in complete eradication of antiproliferative activity (see SI Table 1 and SI Figure 2, compounds **28** and **29**). As shown in Figure 2A,B, we designed and evaluated several other analogs with alternate chloro/nitro substitution patterns (**16**−**19**), but all resulted in significantly less active benzamides when compared to 4-chloro-3-nitrobenzamide analog **10** (EC_{50} = 182 nM). These initial results, with the position of the chlorine substituent *ortho* and *para* to the mesomeric electron-withdrawing nitro and benzamide carbonyl in the most active analog **10**, raised the possibility that nucleophilic aromatic substitution (S_NAr) was important for the activity of these molecules. According to this model, we hypothesized that a nucleophilic amino acid side chain within a benzamide binding protein would displace the 4-chloro substituent via S_NAr, resulting in a covalent bond to the target protein (Figure 2D).

To further evaluate this model, we generated analogs in which the chlorine leaving group was replaced with other leaving groups including fluorine, bromine, or iodine (Figure 2A,C). The activity of **20** (EC_{50} = 818 nM), **10** (EC_{50} = 182 nM), **21** (EC_{50} = 55 nM), and **22** (EC_{50} = 51 nM) positively correlated with the leaving group potential and the size of the halide substituent at position 4. Interestingly, analog **23** bearing 4-OCF_3 was the most potent benzamide tested (EC_{50} = 20 nM).[6] The impact of all these benzamide ring modifications was consistent with a nucleophilic aromatic substitution mediating a covalent compound−protein interaction.

Benzamides Bind Covalently to a Protein p50, Identified as *β*-Tubulin. We developed alkyne-modified chemical probes to visualize potential covalent small molecule protein complexes by SDS-PAGE via a copper-mediated click reaction with a fluorescent azide dye for in-gel detection.[7−9]

https://dx.doi.org/10.1021/acs.jmedchem.0c01482
J. Med. Chem. 2020, 63, 14054−14066

A

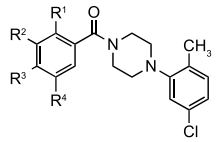

cpd	R^1	R^2	R^3	R^4	IC_{50} (μM)
16	NO_2	H	Cl	H	17.04 (±2.57)
17	Cl	NO_2	H	H	12.44 (±1.35)
10	H	NO_2	Cl	H	0.18 (±0.03)
18	H	NO_2	H	Cl	4.87 (±0.61)
19	H	Cl	NO_2	H	4.68 (±0.47)
20	H	NO_2	F	H	0.82 (±0.07)
21	H	NO_2	Br	H	0.055 (±0.02)
22	H	NO_2	I	H	0.05 (±0.01)
23	H	NO_2	OCF_3	H	0.02 (±0.0004)

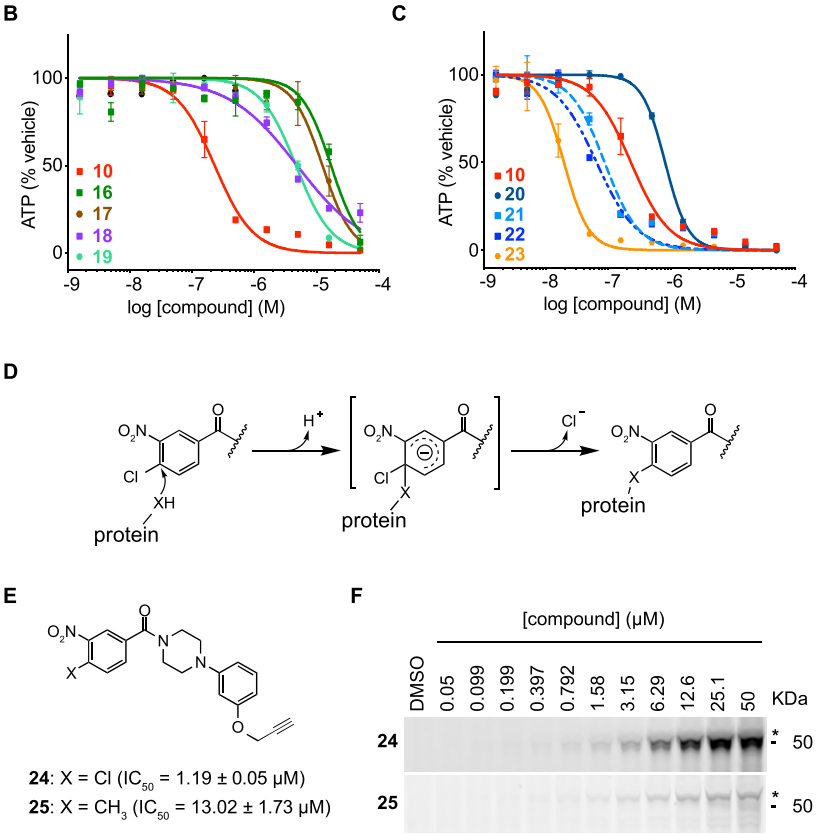

Figure 2. Structure–activity relationships of the 4-chloro-3-nitrobenzamide warhead reveal that benzamides bind covalently to p50 via aromatic nucleophilic substitution. (A) Table with half-maximal inhibitory concentrations (IC_{50}) for benzamide analogs against murine SCLC line 319N1. Standard error is indicated between brackets and is based on $n = 2$ technical replicates. (B and C) Dose–response curves for analogs **10** and **16**–**23** against murine SCLC cell line 319N1. (D) Model for potential covalent cross-linking of the 4-chloro-3-nitrobenzamide warhead with binding protein via nucleophilic aromatic substitution. (E) Benzamide alkyne probe reagents **24** and **25** with half-maximal inhibitory concentrations (IC_{50}) against murine SCLC line 319N1. Standard error is indicated between brackets and is based on $n = 2$ technical replicates. (F) SDS-PAGE gels of fluorescent azide dye-treated cell lysates obtained from 518T2 murine SCLC cells incubated with increasing concentrations of analogs **24** and **25**.

Based on the SAR described in Figure 1, we decided to introduce the alkyne "click" handle in the *meta*-position of the piperazinophenyl ring as a phenolic propargyl ether. Alkyne **24** harbored the benzamide S_NAr warhead, whereas the corresponding alkyne analog **25** was substituted with a methyl group of similar van der Waals radius to chlorine but would not be expected to covalently bind to the target protein (Figure 2E). Consistent with this, methyl-substituted benzamide **25** was 10-fold less active compared to **24** (Figure 2E).

To visualize potential covalently modified proteins, murine SCLC cells were incubated with varying concentrations of either **24** or **25** (from 50 nM to 50 μM). Protein lysates were then subjected to the copper-mediated click reaction using a fluorescent azide dye (Alexa Fluor 532), and protein-probe complexes were visualized using an SDS-PAGE gel. A single dominant 50 kDa protein (hereafter referred as p50) was covalently modified by S_NAr reactive probe **24**, a band which was not observed in lysates incubated with **25** (Figure 2F and SI Figure 3).

Although the above experiments clearly demonstrated that the benzamide probe with an active S_NAr warhead (**24**) was capable of forming an irreversible complex with p50, it remained to be determined whether this interaction was relevant to the anti-cancer activity of these compounds. To address this question in a quantitative fashion, we selected nine benzamide analogs that varied in potency between 51 nM and 4.36 μM in the cell-based phenotypic assay (cytotoxicity against mSCLC cell line 319N1) for a cell-based competition

https://dx.doi.org/10.1021/acs.jmedchem.0c01482
J. Med. Chem. 2020, 63, 14054–14066

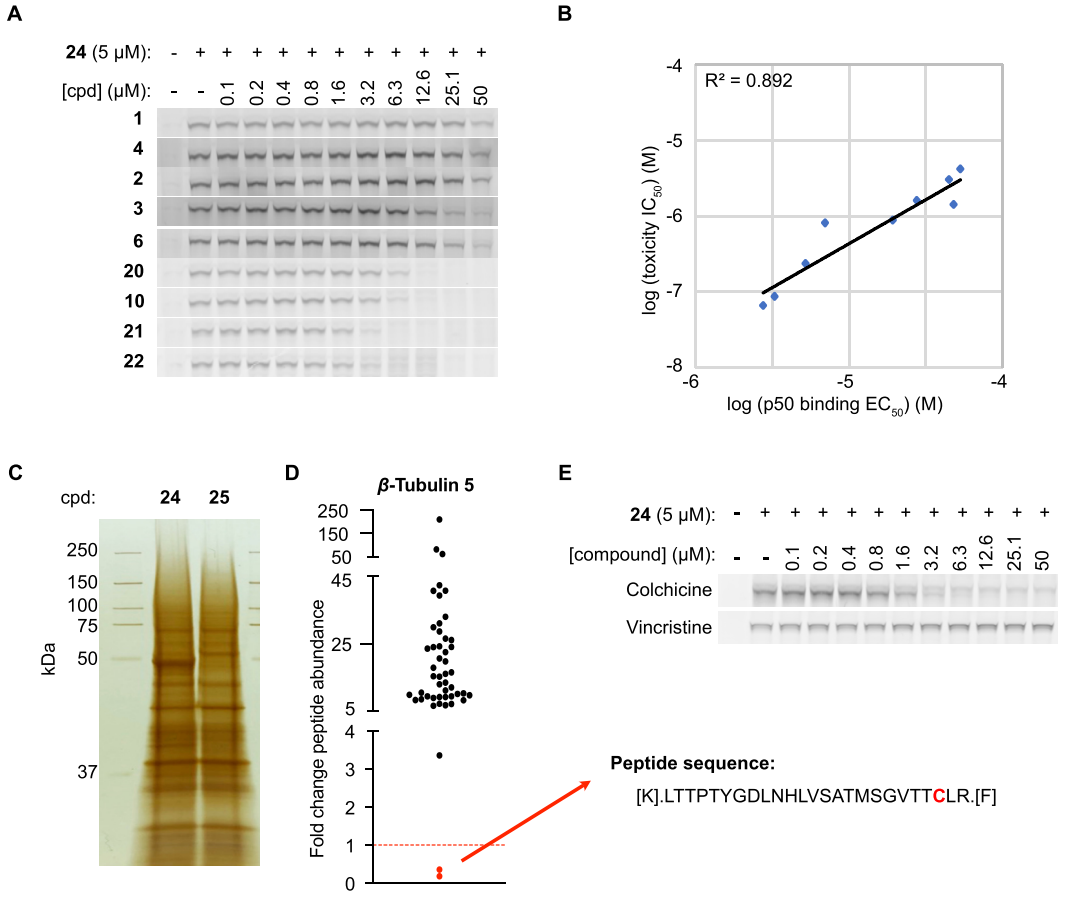

Figure 3. Binding of benzamides to the β-tubulin colchicine site is responsible for toxicity in SCLC cells. (A) SDS-PAGE gels of fluorescent azide dye-treated cell lysates obtained from 518T2 murine SCLC cells incubated with alkyne probe **24** (5 μM) after pre-treatment with increasing concentrations of compounds **1**−**4**, **6**, **10**, and **20**−**22**. (B) Correlation among nine benzamide analogs for toxicity (IC_{50}) and p50 binding (EC_{50}). (C) Silver-stained SDS-PAGE gel of pull-down samples treated with probe **24** or probe **25**. (D) Fold change of β_5 tubulin peptide abundance in sample **24** normalized to sample **25**. (E) SDS-PAGE gels of fluorescent azide dye-treated cell lysates obtained from 518T2 murine SCLC cells incubated with alkyne probe **24** (5 μM) after pre-treatment with increasing concentrations of colchicine or vincristine.

experiment with the clickable alkyne probe **24** in the probe-binding assay (Figure 3A and SI Figure 4). We identified a positive correlation between the cellular toxicity (IC_{50}) of these nine analogs (see Figures 1A and 2A) and their respective ability to displace alkyne probe **24** (EC_{50}) with an R^2 value of 0.8895 (Figure 3B). These results were consistent with p50 binding being responsible for the anti-cancer activity of this series of benzamide analogs.

To enable identification of p50 using chemical probe−protein precipitation and mass spectrometry-based proteomics, the cross-linking experiment was repeated on a larger scale. After incubating cells with covalent alkyne probe **24** or with non-covalent probe **25**, lysates were prepared and clicked to a biotin azide (instead of a fluorescent azide). The resulting biotin−protein−probe complexes were precipitated with streptavidin beads followed by boiling the beads. Proteins in the eluate were analyzed by SDS-PAGE and visualized using silver staining, confirming that p50 was pulled down in the sample treated with covalent probe **24** but not in the sample with compound **25** (Figure 3C). Shotgun LC−MS/MS analysis identified β-tubulin as the only protein enriched in the probe **24** treated sample (SI Table 2), of which β-tubulin isoform 5 (Tubb5; β_5 tubulin) was the most enriched (12.95-fold) of the various isoforms.

Benzamides Bind β-Tubulin in the Colchicine Binding Pocket and Alter Microtubule Dynamics. Notably, when focusing on the peptide counts for Tubb5 (β_5 tubulin), we found that there was one single peptide (aa217-241) that was depleted from the probe-only treated sample (Figure 3D). We hypothesized that this peptide was depleted from the MS dataset due to a mass shift resulting from a covalent modification with the probe. The 217-241 peptide contained a single cysteine, raising the possibility that this residue acted as the nucleophile in the S_NAr reaction with the probe. There have been at least two other small molecules reported to covalently modify β-tubulin at Cys239. T0070907 was a compound initially identified as an inhibitor of PPARγ via covalent modification of Cys313.[10] Subsequently, T0070907 was shown to also induce tubulin degradation[11,12] followed by a report by Yang et al. showing covalent modification of Cys239 of β-tubulin via displacement of the chlorine *para* to the nitro group in the 2-Cl-5-nitrobenzamide moiety of T0070907.[13] Another compound, T138067 was also shown to bind covalently to β-tubulin through Cys239 by displacement of the *para*-fluorine in the pentafluorophenylsulfonamide warhead of T138067.[14,15]

Colchicine is a natural product that binds β-tubulin in a pocket located near the $\alpha\beta$-tubulin heterodimer interface. Cys239 lies within the colchicine binding pocket of β-tubulin

https://dx.doi.org/10.1021/acs.jmedchem.0c01482
J. Med. Chem. 2020, 63, 14054−14066

and has been shown to be important for colchicine activity.[16] Because our data suggested that benzamides interact with Cys239 within the colchicine binding pocket, we performed a competition experiment between covalent benzamide probe **24** and colchicine. As depicted in Figure 3E, colchicine was able to displace binding of alkyne probe **24** (5 μM) to p50 in a dose-dependent manner with an EC_{50} of 2.8 μM. Also, no such probe competition was observed with vincristine, a microtubule-destabilizing agent that acts at a site distinct from the colchicine site (Figure 3E). This data provided additional evidence that benzamides bound β-tubulin within the colchicine binding pocket.

Colchicine and other drugs that target β-tubulin impair microtubule dynamics and cause cell cycle arrest at the G_2/M transition due to the impairment of chromosome segregation during mitosis.[17] As expected, cell cycle analysis indicated that mSCLC cells treated with 300 nM colchicine or benzamide analog **21** (IC_{50} = 69 nM) for 24 h induced G_2/M cell cycle arrest (Figure 4A).

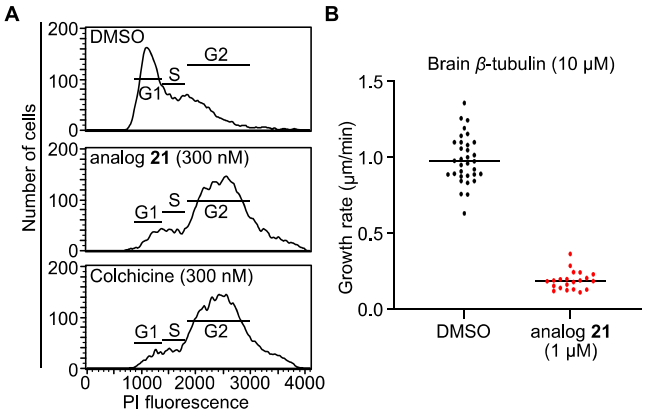

Figure 4. Benzamide analog **21** inhibits microtubule growth and induces G2/M cell cycle arrest. (A) Cell cycle analysis by flow cytometry of 518T2 cells treated with DMSO, analog **21** (300 nM), or colchicine (300 nM) for 24 h. (B) Quantification of the growth rate of microtubules using brain tubulin from samples treated with DMSO (33 microtubules quantified) and samples treated with analog **21** (21 microtubules quantified); n = 1 trial.

Microtubules are dynamic structures in the cell that undergo phases of growth and shrinkage in a phenomenon called dynamic instability.[18] Drugs that bind the colchicine binding pocket of β-tubulin alter these dynamics and destabilize microtubule fibers.[19] We therefore performed *in vitro* microtubule formation assays to assess the impact of benzamide analog **21** on microtubule dynamics. Compared to control, the growth of bovine brain microtubules was reduced by approximately 80% in the presence of analog **21** even at 10:1 (tubulin/compound) ratio (Figure 4B and SI Figure 5A).

Targeting the β_3 Tubulin Isoform with Aldehyde-Modified Benzamides. A common mechanism of resistance to taxanes, the most commonly used microtubule-targeting agent for cancer therapy, is the overexpression of β_3 tubulin (encoded by TUBB3) in which Arg277 replaces Ser277 in the M loop, greatly reducing the binding of taxane agents.[20,21] Therefore, agents that target a site distinct from where taxanes bind could have translational potential. Given that the benzamides described herein target the colchicine site, we considered whether these might be active against β_3 tubulin overexpressing cancers.[19,22] However, the isoform switch to β_3 tubulin indirectly impacts the colchicine binding pocket because TUBB3 encodes serine at position 239, rather than cysteine. Given that benzamides covalently modified β-tubulin potentially via Cys239 (Figure 3D), their binding affinity for the Ser239 containing β_3 isoform could be dramatically impaired. Indeed, our proteomic datasets indicated that β_3 tubulin was enriched only 3-fold compared to the average 9.2-fold enrichment for the other isoforms of β-tubulin (β_{2A}, β_{2B}, β_{4A}, β_{4B}, and β_5), which harbor a cysteine at position 239 (SI Table 2). Consistent with this observation, benzamide analog **21** (up to 10 μM) failed to impair the *in vitro* microtubule growth rate of tubulin preparations using human recombinant β_3 tubulin (Figure 5B and SI Figure 5B),[23] whereas this same compound (at 1 μM) dramatically affected the growth of brain tubulin containing primarily the Cys239 containing β-tubulin isoforms (Figure 4B).

We therefore set out to design an analog that would engage serine 239 in hemiacetal formation with an appropriately placed aldehyde. Importantly, it was anticipated that such an

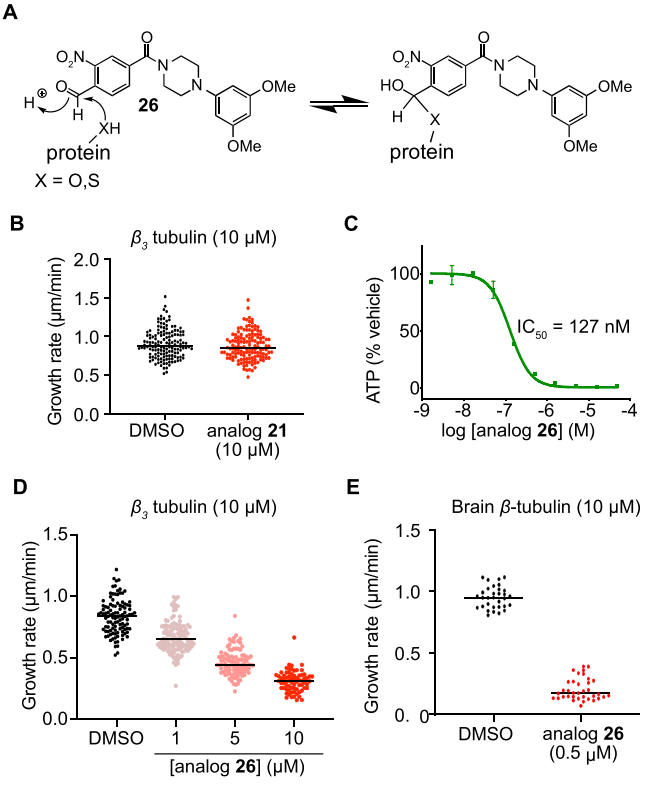

Figure 5. Formyl-substituted benzamide analog **26** enables the inhibition of the Ser239-containing β_3 tubulin isoform. (A) Model for hemiacetal formation of benzaldehyde analog **26** with serine or cysteine residues. (B) Quantification of the growth rate of β_3 tubulin microtubules treated with DMSO (n = 131 microtubules quantified over three trials) or analog **21** (n = 126 microtubules quantified over three trials). (C) Dose–response curve of compound **26** in murine SCLC cell line 319N1. (D) Quantification of the growth rate of microtubules using β_3 tubulin treated with DMSO (n = 107 microtubules quantified over two trials) or analog **26** at 1 μM (n = 119 microtubules quantified over two trials), 5 μM (n = 102 microtubules quantified over two trials), and 10 μM (n = 71 microtubules quantified over two trials). (E) Quantification of the growth rate of microtubules using brain tubulin from samples treated with DMSO (n = 32 microtubules quantified over one trial) or analog **26** (n = 36 microtubules quantified over one trial).

https://dx.doi.org/10.1021/acs.jmedchem.0c01482
J. Med. Chem. 2020, 63, 14054−14066

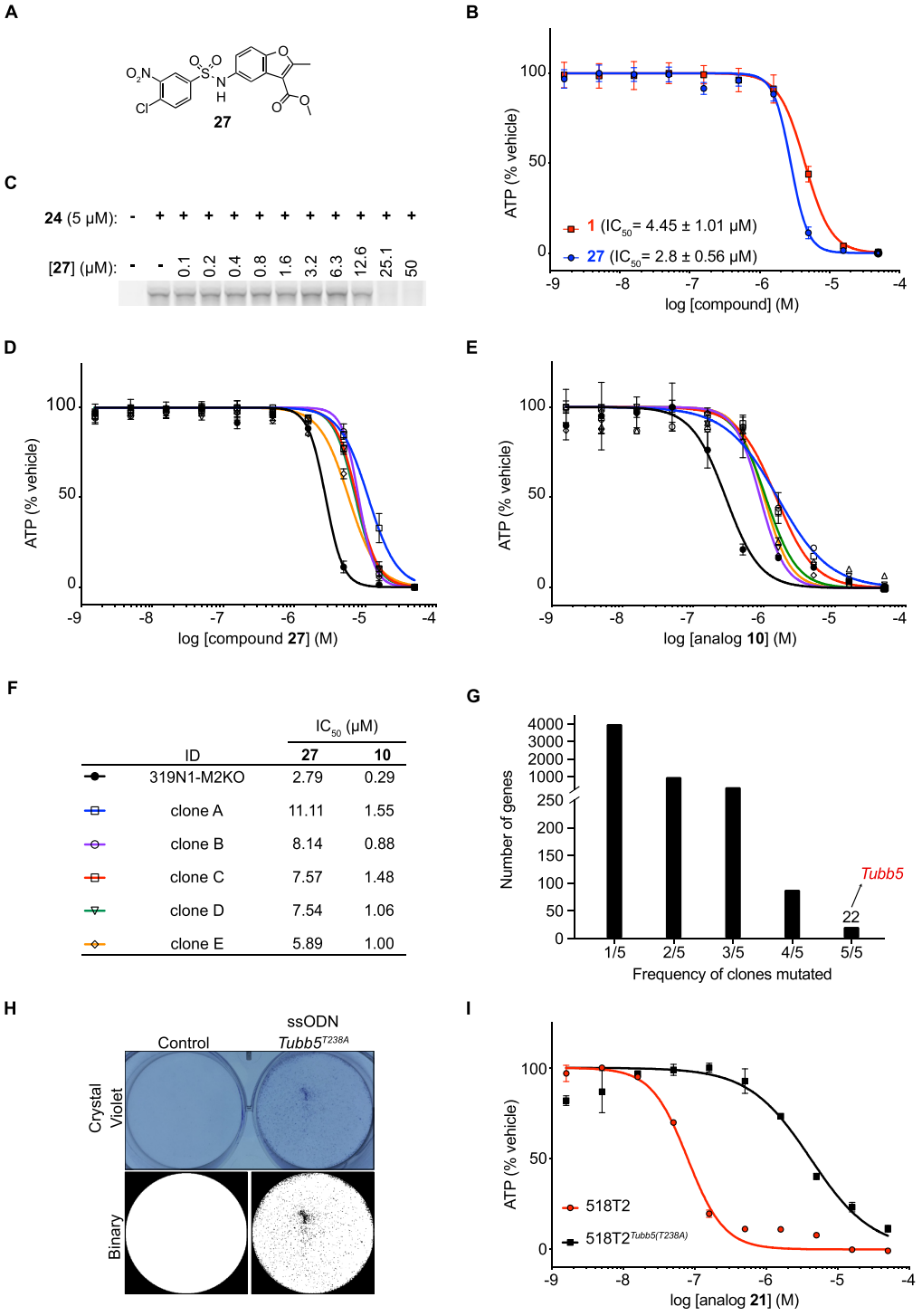

Figure 6. *Tubb5*^{T238A} compound-resistant allele identified by forward genetics is sufficient to confer benzamide resistance in murine SCLC cells. (A) Structure of compound **27**. (B) Dose−response curve of compounds **1** and **27** against a murine SCLC cell line 319N1. Standard error is indicated between brackets and is based on $n = 2$ technical replicates. (C) SDS-PAGE gels of fluorescent azide dye-treated cell lysates obtained from 518T2 murine SCLC cells incubated with alkyne probe **24** (5 μM) after pre-treatment with increasing concentrations of compound **27**. (D and E) Dose−response curves of compounds **27** and **10** in parental *Msh2*-deficient 319N1-M2KO cell line and resistant clones A−E. (F) Table with half-maximal inhibitory concentrations (IC_{50}) for benzamide analogs **10** and **27** against the parental 319N1-M2KO cell line and five resistant clones A−E. (G) *Tubb5* is one of the only 22 genes recurrently mutated in all five resistant clones. (H) Crystal violet staining of murine SCLC (518T2) cells edited in *Tubb5* harboring the T238A mutation (top). Binary images from crystal violet images enable clearer representation of alive cells in the *Tubb5* (T238A) sample (bottom). (I) Dose−response curves of analog **21** in 518T2 cells and 518T2-*Tubb5*^{T238A} cells.

analog would retain the capacity to capture Cys239 isoforms in the form of a hemithioacetal instead of via S_NAr (Figure 5A). Gratifyingly, replacing the halide substituent in the benzamide ring with a formyl group led to analog **26** that retained potent anti-cancer activity against 319N1 mSCLC cells (EC_{50} = 127 nM) (Figure 5C). Consistent with our hypothesis, benzaldehyde **26** dose-dependently altered the dynamics of microtubules composed exclusively of β_3 tubulin in a dose-

https://dx.doi.org/10.1021/acs.jmedchem.0c01482
J. Med. Chem. 2020, 63, 14054−14066

dependent manner (Figure 5D). Microtubule growth rate was reduced from 0.83 μm/min in the DMSO control to 0.67 μm/min with analog **26** (10:1 ratio β_3 tubulin/**27**). Further growth rate reduction was achieved at higher analog **26** concentrations, reaching 0.31 μm/min at 10 μM (Figure 5D and SI Figure 5B). Importantly, benzaldehyde **26** also potently reduced the growth of microtubules in preparations of bovine brain tubulin, which is composed primarily of Cys239-containing β-tubulin isoforms (Figure 5E and SI Figure 5C). In conclusion, aldehyde analogs such as **26** target both Cys239 and Ser239 isoforms, presumably via hemiacetal/hemithioacetal formation, which lays out a potential chemical strategy to target cancers that acquire resistance through β_3 tubulin overexpression.

Competition with Benzamide Probe 24 and Forward Genetics Identify Another HTS Hit That Binds β-Tubulin at the Colchicine Binding Site. Given that microtubules are frequently targeted by small molecules, by design or unintended,[16,24,25] we contemplated that benzamide probe **24** might be useful to identify other toxins that act through binding at the β-tubulin colchicine site. When we examined our mSCLC HTS hit list, a chloronitrobenzenesulfonamidobenzofuran (**27**, IC_{50} = 2.8 μM, Figure 6A,B) was flagged as containing structural features essential for nucleophilic aromatic substitution. As shown in Figure 6C, sulfonamide **27** displaced probe **24** from p50 in a dose-responsive manner. This result is consistent with the notion that microtubules are the mechanistic target of compound **27**, presumably via covalent capture of Cys239 β-tubulin isoforms.

Simultaneous to our efforts to develop probe reagents for biochemical target identification studies, we utilized a forward genetics target identification strategy that we recently reported.[26] Deletion of the DNA mismatch repair protein MSH2 using CRISPR-Cas9 is sufficient to induce hypermutation in human and murine cancer cell lines. The increased mutation frequency facilitates the emergence of clones that harbor compound-resistant alleles in the target of small molecule cytotoxins. We therefore generated a barcoded (20-nucleotide barcode) clonal mSCLC cell line (319N1-M2KO) using a lentiviral vector encoding blasticidin resistance. We successfully generated and validated independent barcoded clones resistant to sulfonamide **27**. We performed compound selections using **27** at five concentrations close to the lethal dose, as determined by 1 week of compound exposure (EC_{100}^{1wk}). Following 2 weeks of compound selection, compound-resistant colonies emerged and were expanded. To confirm *in vitro* resistance, we determined the IC_{50} for five independent 319N1-M2KO clones (A–E) and confirmed that all were resistant to **27** (IC_{50} > 2-fold change, Figure 6D,F). Interestingly, all five clones were cross-resistant to benzamide **10**, suggesting a shared molecular target or resistance mechanism (IC_{50} > 2.5-fold-change, Figure 6E,F). The same clones were not cross-resistant to etoposide, suggesting that general resistance mechanisms were not responsible for the emergence of these clones in response to selection with sulfonamide **27** (SI Figure 6).

To identify recurrently mutated genes across multiple resistant clones, all five sulfonamide **27** resistant clones were subjected to exome sequencing. We identified 22 genes mutated in five out of five clones (Figure 6G). Among these was a common *Tubb5* mutation (712A > G) that resulted in a T238A (Thr > Ala) amino acid substitution immediately adjacent to the Cys239. It was of interest that the T238A mutation had previously been identified in yeast tubulin (TUB2) as a resistance mutation to benomyl, a microtubule inhibitor that also binds at the colchicine binding site.[27,28] To our knowledge, this mutation had not been previously identified in mammalian cells, but this nonetheless raised the possibility that T238A mediated resistance to the benzamide and sulfonamide compound reported here.

Because multiple recurrent mutations existed in each clone, we sought to confirm that the T238A mutation was sufficient to confer resistance to benzamides. We engineered the T238A mutation into 518T2 mSCLC cells using CRISPR/Cas9. After transfection with Cas9 protein-sgRNA complexes targeting *Tubb5* with an oligonucleotide repair template encoding the T238A mutation and a sham control, we selected cells with benzamide **21** at 400 nM for 2 weeks. To visualize compound resistant clones, plates were stained with crystal violet. Emerging clones were observed under the $Tubb5^{T238A}$ condition, whereas no clones were visible under the control condition (Figure 6H). Compound resistance to analog **21** was confirmed in 518T2$^{Tubb5^{T238A}}$ cells compared to parental 518T2 cells (Figure 6I). Thus, introduction of a single T238A mutation in *Tubb5* in murine SCLC cell lines was sufficient to endow resistance to the benzamides (**10** and **21**) and arylsulfonamide **27**. This result established a causal relationship between the mutation and compound resistance.

CHEMISTRY

Compounds **1**, **7**, **11**, **12**, and **27**–**29** were commercially available. As shown in Scheme 1, reaction of 4-chloro-3-nitrobenzoyl chloride with a collection of arylpiperazines **I** in the presence of triethylamine delivered benzamide analogs **2**–**6**, **8**–**10**, and **13**–**15**. Analogs **16**–**23** and **26** were obtained via condensation of benzoic acid derivatives **II** with arylpiperazines **I** mediated by EDC as the dehydrating agent and DMAP as the catalyst. Benzamide analogs **24** and **25** were obtained from the corresponding phenolic benzamide intermediates via an additional propargylation with propargyl bromide and potassium carbonate in dimethylformamide.

Scheme 1. Synthesis of Benzamides[a]

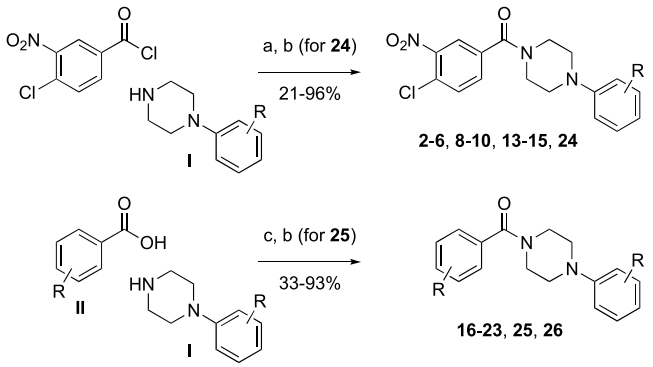

[a]Reagents and conditions: (a) NEt_3, THF, rt; (b) (for **24** and **25**) propargyl bromide, K2CO3, DMF; (c) EDC·HCl, DMAP, DMF, rt.

CONCLUSIONS

Here, we disclosed a multipronged approach to establish the mode of action of benzamides with anti-cancer activity to SCLC. Through medicinal chemistry, probe reagent development, and biochemical pull-down methods, we established that

https://dx.doi.org/10.1021/acs.jmedchem.0c01482
J. Med. Chem. 2020, 63, 14054–14066

these benzamides target β-tubulin through the colchicine binding pocket using a nucleophilic aromatic substitution to covalently modify cysteine 239. Consistent with this mechanism of action, we demonstrated that these cytotoxins impair microtubule dynamics *in vitro* and induce cell cycle arrest at the G_2/M transition. In addition, β-tubulin isoforms (including β_3 tubulin) that encode serine at position 239 exhibited intrinsic resistance to the benzamide compounds as a result of the reduced nucleophilicity of serine compared to cysteine. We reported a strategy to engage serine-bearing β-tubulin isoforms by developing a benzaldehyde analog that targets serine 239 through hemiacetal formation. Forward genetics screening with a cell line harboring engineered DNA mismatch repair deficiency identified a compound-resistant allele in threonine 238 (Thr238Ala) that was sufficient to encode resistance to anti-cancer toxins bearing the chloronitrobenzene S_NAr warhead.

β-tubulin is a well-validated therapeutic target of several classes of anti-cancer natural products and small molecules. However, β-tubulin is also increasingly identified as an unwanted off-target of small molecules purported to act on other protein targets. Here, we demonstrated the potential of our cell-based probe competition binding assay and expect that the disclosed benzamide probes will prove useful in drug discovery and development to identify compounds with the capacity, by design or not, to bind β-tubulin.

EXPERIMENTAL SECTION

General Methods for Chemistry. Unless otherwise specified, all commercially available reagents were used as received. Compound **1** was purchased from ChemBridge (#5348909). Compounds **7**, **11**, and **28**−**29** were purchased from ChemDiv (#Y031-8281, #Y031-8282, #Y030-0278, and #Y031-8034). Compound **27** was purchased from Princeton BioMolecular Research (#OSSK_101609). Compound **12** was purchased from Enamine (#Z30011284). All reactions using dried solvents were carried out under an atmosphere of argon in flame-dried glassware with magnetic stirring. A dry solvent was dispensed from a solvent purification system that passes the solvent through two columns of dry neutral alumina. Silica gel chromatographic purifications were performed by flash chromatography with a silica gel (Sigma, grade 60, 230−400 mesh) packed in glass columns (the eluting solvent was determined by thin-layer chromatography, TLC), or with an Isco Combiflash system using Redisep Rf Flash columns with size ranging from 4 to 80 g. Analytical TLC was performed on glass plates coated with a 0.25 mm silica gel using UV or by iodide or $KMnO_4$ staining for visualization. Routine ^{1}H and proton-decoupled ^{13}C NMR spectra were obtained on an Agilent 400 MHz NMR spectrometer. Chemical shifts (δ) are reported in parts per million (ppm) from low to high field relative to the residual solvent. Multiplicities are given as s (singlet), bs (broad singlet), d (doublet), t (triplet), q (quartet), dd (doublet of doublets), dt (doublet of triplets), and m (multiplet). HRMS data were obtained from the Shimadzu Center for Advanced Analytical Chemistry (SCAAC) at U.T. Arlington. All purchased and synthetic compounds exhibited between 95 and 99% purity as determined by LC−MS analysis performed on an Agilent 1290 HPLC system using an Eclipse XDB-C18 column (4.6 × 150 mm, 5 μm; Agilent) that was coupled to an Agilent 6130 mass spectrometer run in ESI mode in both positive and negative ionization with a scan range of 100−1100 m/z. Liquid chromatography was carried out at a flow rate of 0.5 mL/min at 20 °C with a 5 μL injection volume using the gradient elution with aqueous acetonitrile containing 0.1% formic acid. The gradient was adjusted based on the different polarities of different compounds.

General Procedure A for the Preparation of Benzamides from 4-Chloro-3-nitrobenzoyl Chloride and Arylpiperazines I. A solution of 4-chloro-3-nitrobenzoyl chloride, arylpiperazine **I**, and triethylamine in THF was stirred at room temperature for 16 h. The concentration of the reaction mixture followed by flash chromatography (gradient of 0−50% EtOAc in hexane) gave the corresponding benzamide.

General Procedure B for the Preparation of Benzamides from Substituted Benzoic Acids II and Arylpiperazines I. To a solution of arylpiperazine **I**, benzoic acid derivative **II**, and DMAP in DMF was added EDC·HCl at rt. The resulting reaction mixture was stirred for 16 h. Flash chromatography (gradient of 0−40% EtOAc in hexane) gave the corresponding benzamide.

(4-Chloro-3-nitrophenyl)(4-(2-chlorophenyl)piperazin-1-yl)-methanone (2). Prepared according to Procedure A using 4-chloro-3-nitrobenzoyl chloride (75.0 mg, 0.34 mmol), 1-(2-chlorophenyl)-piperazine HCl salt (104.0 mg, 0.44 mmol), and Et_3N (0.90 mL, 6.45 mmol) in THF (4 mL). Yield 89 mg (68%) as a light-yellow solid. ^{1}H NMR (400 MHz, $CDCl_3$) δ 7.97 (d, J = 1.6 Hz, 1H), 7.66−7.55 (m, 2H), 7.36 (dd, J = 8.2, 1.5 Hz, 1H), 7.26−7.16 (m, 1H), 7.05−6.96 (m, 2H), 3.94 (bs, 2H), 3.60 (bs, 2H), 3.22−2.92 (m, 4H); ^{13}C NMR (101 MHz, $CDCl_3$) δ 166.8, 148.3, 147.7, 135.5, 132.3, 131.8, 130.75, 128.9, 128.51, 127.79, 124.66, 124.57, 120.62, 51.58, 50.92, 48.15, 42.7; HRMS calculated for $C_{17}H_{15}Cl_2N_3O_3$ $[M + H]^+$ 380.0563, found 380.0541.

(4-Chloro-3-nitrophenyl)(4-(3-methoxyphenyl)piperazin-1-yl)methanone (3). Prepared according to Procedure A using 4-chloro-3-nitrobenzoyl chloride (106.0 mg, 0.48 mmol), 1-(3-methoxyphenyl)piperazine (251.0 mg, 1.31 mmol), and Et_3N (0.30 mL, 2.15 mmol) in THF (4 mL). Yield 146 mg (80%) as a light-yellow solid. ^{1}H NMR (400 MHz, $CDCl_3$) δ 7.94 (d, J = 1.7 Hz, 1H), 7.64−7.55 (m, 2H), 7.17 (t, J = 8.0 Hz, 1H), 6.56−6.47 (m, 1H), 6.47−6.41 (m, 2H), 3.88 (s, 2H), 3.76 (s, 3H), 3.57 (d, J = 8.9 Hz, 2H), 3.32−3.01 (m, 4H); ^{13}C NMR (101 MHz, $CDCl_3$) δ 166.65, 160.6, 152.0, 147.7, 135.3, 132.3, 131.9, 130.0, 128.5, 124.7, 109.4, 105.5, 103.3, 55.2, 49.7, 49.3, 47.6, 42.4; HRMS calculated for $C_{18}H_{18}ClN_3O_4$ $[M + H]^+$ 376.1059, found 376.1042.

(4-Chloro-3-nitrophenyl)(4-(*m*-tolyl)piperazin-1-yl)-methanone (4). Prepared according to Procedure A using 4-chloro-3-nitrobenzoyl chloride (75.0 mg, 0.34 mmol), 1-(3-methylphenyl)-piperazine (124.0 mg, 0.70 mmol), and Et_3N (0.30 mL, 2.15 mmol) in THF (4 mL). Yield 110 mg (89%) as light-yellow gummy solid. ^{1}H NMR (400 MHz, $CDCl_3$) δ 7.97 (d, J = 1.7 Hz, 1H), 7.66−7.57 (m, 2H), 7.17 (t, J = 7.9 Hz, 1H), 6.78−6.70 (m, 3H), 3.91 (bs, 2H), 3.58 (bs, 2H), 3.19 (m, 4H), 2.33 (s, 3H); ^{13}C NMR (101 MHz, $CDCl_3$) δ 166.7, 150.7, 147.8, 139.1, 135.4, 132.3, 131.9, 129.15, 128.6, 124.7, 121.85, 117.75, 114.0, 49.9, 47.8, 42.5, 21.75; HRMS calculated for $C_{18}H_{18}ClN_3O_3$ $[M + H]^+$ 360.1109, found 360.1090.

(4-Chloro-3-nitrophenyl)(4-(2,5-dimethylphenyl)piperazin-1-yl)methanone (5). Prepared according to Procedure A using 4-chloro-3-nitrobenzoyl chloride (75.0 mg, 0.34 mmol), 1-(2,5-dimethylphenyl)piperazine (122.0 mg, 0.64 mmol), and Et_3N (0.60 mL, 4.30 mmol) in THF (4 mL). Yield 122 mg (96%) as a light-yellow thick oil. ^{1}H NMR (400 MHz, $CDCl_3$) δ 7.99 (d, J = 1.5 Hz, 1H), 7.63 (d, J = 1.2 Hz, 2H), 7.09 (d, J = 7.6 Hz, 1H), 6.88−6.79 (m, 2H), 4.04−3.81 (m, 2H), 3.59 (bs, 2H), 3.03−2.82 (m, 4H), 2.31 (s, 3H), 2.28 (s, 3H); ^{13}C NMR (101 MHz, $CDCl_3$) δ 166.8, 150.35, 147.8, 136.4, 135.6, 132.3, 131.9, 131.1, 129.4, 128.45, 124.7, 124.65, 120.1, 52.1, 51.7, 48.5, 43.05, 21.2, 17.4; HRMS calculated for $C_{19}H_{20}ClN_3O_3$ $[M + H]^+$ 374.1266, found 374.1242.

(4-(3-Bromophenyl)piperazin-1-yl)(4-chloro-3-nitrophenyl)-methanone (6). Prepared according to Procedure A using 4-chloro-3-nitrobenzoyl chloride (49.0 mg, 0.22 mmol), 1-(3-bromophenyl)-piperazine (55.0 mg, 0.23 mmol), and Et_3N (0.10 mL, 0.72 mmol) in THF (2 mL). Yield 81 mg (92%) as a white solid. ^{1}H NMR (400 MHz, $CDCl_3$) δ 7.96 (d, J = 1.8 Hz, 1H), 7.66−7.56 (m, 2H), 7.12 (t, J = 8.0 Hz, 1H), 7.06−6.98 (m, 2H), 6.82 (ddd, J = 8.3, 2.3, 1.0 Hz, 1H), 3.74 (m, 9 Hz, 4H), 3.38−3.03 (m, 4H); ^{13}C NMR (101 MHz, $CDCl_3$) δ 166.7, 151.8, 147.8, 135.1, 132.4, 131.8, 130.6, 128.7, 124.7, 123.5, 123.3, 119.55, 115.2, 49.2, 47.5, 42.3; HRMS calculated for $C_{17}H_{15}BrClN_3O_3$ $[M + H]^+$ 424.0058, found 424.0030.

3-(4-(4-Chloro-3-nitrobenzoyl)piperazin-1-yl)benzonitrile (8). Prepared according to Procedure A using 4-chloro-3-nitrobenzoyl chloride (100.0 mg, 0.45 mmol), 1-(3-cyanophenyl)piperazine (172.0

https://dx.doi.org/10.1021/acs.jmedchem.0c01482
J. Med. Chem. 2020, 63, 14054−14066

mg, 0.92 mmol), and Et_3N (0.3 mL, 2.15 mmol) in THF (4 mL). Yield 135 mg (80%) as a light-yellow gummy solid. ^1H NMR (400 MHz, $CDCl_3$) δ 7.94 (t, J = 1.2 Hz, 1H), 7.59 (d, J = 1.5 Hz, 2H), 7.37−7.26 (m, 1H), 7.14−7.05 (m, 3H), 4.08−3.47 (m, 4H), 3.22 (bs, 4H); ^{13}C NMR (101 MHz, $CDCl_3$) δ 166.7, 150.7, 147.7, 135.1, 132.4, 131.9, 130.15, 128.6, 124.7, 123.55, 120.6, 119.1, 119.05, 113.0, 48.6, 47.3, 42.1; HRMS calculated for $C_{18}H_{15}ClN_4O_3$ $[M + H]^+$ 371.0905, found 371.0882.

(4-Chloro-3-nitrophenyl)(4-(2,5-dichlorophenyl)piperazin-1-yl)methanone (9). Prepared according to Procedure A using 4-chloro-3-nitrobenzoyl chloride (65.0 mg, 0.30 mmol), 1-(2,5-dichlorophenyl)piperazine (103.0 mg, 0.34 mmol), and Et_3N (0.30 mL, 2.20 mmol) in THF (3 mL). Yield 26 mg (21%) as a light-yellow solid. ^1H NMR (400 MHz, $CDCl_3$) δ 7.97 (d, J = 1.8 Hz, 1H), 7.67−7.57 (m, 2H), 7.30 (d, J = 8.4 Hz, 1H), 7.05−6.95 (m, 2H), 3.95 (bs, 2H), 3.61 (bs, 2H), 3.25−2.91 (m, 4H); ^{13}C NMR (101 MHz, $CDCl_3$) δ 166.9, 149.3, 147.9, 135.4, 133.4, 132.5, 131.9, 131.6, 128.8, 127.3, 124.75, 124.6, 121.2, 51.5, 50.9, 48.1, 42.7; HRMS calculated for $C_{17}H_{15}C_{l3}N_3O$ $[M + H]^+$ 414.0174, found 414.0155.

(4-(5-Chloro-2-methylphenyl)piperazin-1-yl)(4-chloro-3-nitrophenyl)methanone (10). Prepared according to Procedure A using 4-chloro-3-nitrobenzoyl chloride (77.0 mg, 0.35 mmol), 1-(5-chloro-2-methylphenyl)piperazine (121.0 mg, 0.57 mmol), and Et_3N (0.30 mL, 2.15 mmol) in THF (4 mL). Yield 140 mg (68%) as a light-yellow oil. ^1H NMR (400 MHz, $CDCl_3$) δ 7.96 (d, J = 1.6 Hz, 1H), 7.61 (d, J = 2.0 Hz, 2H), 7.09 (d, J = 8.0 Hz, 1H), 7.02−6.90 (m, 2H), 3.90 (bs, 2H), 3.57 (bs, 2H), 3.10−2.71 (m, 4H), 2.26 (s, 3H); ^{13}C NMR (101 MHz, $CDCl_3$) δ 166.8, 151.5, 147.7, 135.4, 132.3, 132.2, 131.85, 131.8, 131.0, 128.5, 124.6, 123.9, 119.8, 51.7, 51.5, 48.2, 42.8, 17.4; HRMS calculated for $C_{18}H_{17}C_{l2}N_3O_3$ $[M + Na]^+$ 416.0539, found 416.0512.

(4-Chloro-3-nitrophenyl)(4-(2,4-difluorophenyl)piperazin-1-yl)methanone (13). Prepared according to Procedure A using 4-chloro-3-nitrobenzoyl chloride (75.0 mg, 0.34 mmol), 1-(2,4-difluorophenyl)piperazine (111.0 mg, 0.56 mmol), and Et_3N (0.60 mL, 4.30 mmol) in THF (4 mL). Yield 92 mg (71%) as a light-yellow gummy solid. ^1H NMR (400 MHz, $CDCl_3$) δ 7.95 (d, J = 1.7 Hz, 1H), 7.68−7.55 (m, 2H), 6.89 (td, J = 9.9, 9.4, 5.7 Hz, 1H), 6.80 (dtt, J = 8.1, 5.1, 3.0 Hz, 2H), 3.92 (bs, 2H), 3.59 (bs, 2H), 3.03 (m, 4H); ^{13}C NMR (101 MHz, $CDCl_3$, including ^{19}F-coupling peaks) δ 166.7, 159.7, 159.6, 157.2, 157.1, 157.1, 156.95, 154.6, 154.5, 147.75, 135.8, 135.8, 135.75, 135.7, 135.3, 132.3, 131.8, 128.6, 124.6, 120.2, 120.1, 120.1, 120.0, 111.1, 111.03, 110.85, 110.8, 105.2, 104.92, 104.91, 104.7, 51.3, 50.6, 47.95, 42.55; HRMS calculated for $C_{17}H_{14}ClF_2N_3O_3$ $[M + H]^+$ 382.0765, found 382.0742.

(4-Chloro-3-nitrophenyl)(4-(2,4-dimethylphenyl)piperazin-1-yl)methanone (14). Prepared according to Procedure A using 4-chloro-3-nitrobenzoyl chloride (76 mg, 0.34 mmol), 1-(2,4-dimethylphenyl)piperazine (122.0 mg, 0.64 mmol), and Et_3N (0.30 mL, 2.15 mmol) in THF (4 mL). Yield 120 mg (93%) as a light-yellow oil. ^1H NMR (400 MHz, $CDCl_3$) δ 7.99 (t, J = 1.2 Hz, 1H), 7.63 (d, J = 1.3 Hz, 2H), 7.03 (d, J = 2.2 Hz, 1H), 6.99 (dd, J = 8.1, 2.1 Hz, 1H), 6.91 (d, J = 8.1 Hz, 1H), 3.92 (bs, 2H), 3.71−3.42 (m, 2H), 2.91 (m, 4H), 2.30 (s, 3H), 2.29 (s, 3H); ^{13}C NMR (101 MHz, $CDCl_3$) δ 166.75, 148.1, 147.8, 135.6, 133.6, 132.6, 132.3, 132.0, 131.9, 128.45, 127.2, 124.7, 119.2, 52.25, 51.7, 48.5, 43.1, 20.7, 17.65; HRMS calculated for $C_{19}H_{20}ClN_3O_3$ $[M + H]^+$ 374.1266, found 374.1241.

(4-Chloro-3-nitrophenyl)(4-(4-methoxyphenyl)piperazin-1-yl)methanone (15). Prepared according to Procedure A using 4-chloro-3-nitrobenzoyl chloride (75.0 mg, 0.34 mmol), 1-(4-methoxyphenyl)piperazine (120.0 mg, 0.62 mmol), and Et_3N (0.60 mL, 4.30 mmol) in THF (4 mL). Yield 65 mg (51%) as a light-yellow solid. ^1H NMR (400 MHz, $CDCl_3$) δ 7.96 (d, J = 1.8 Hz, 1H), 7.68−7.54 (m, 2H), 6.89 (d, J = 9.2 Hz, 2H), 6.84 (d, J = 9.0 Hz, 2H), 4.03−3.80 (m, 2H), 3.76 (s, 3H), 3.57 (bs, 2H), 3.07 (m, 4H); ^{13}C NMR (101 MHz, $CDCl_3$) δ 166.65, 154.6, 147.75, 144.9, 135.4, 132.3, 131.8, 128.6, 124.6, 119.1, 114.55, 55.5, 51.3, 50.9, 47.9, 42.6; HRMS calculated for $C_{18}H_{18}ClN_3O_4$ $[M + H]^+$ 376.1059, found 376.1045.

(4-(5-Chloro-2-methylphenyl)piperazin-1-yl)(4-chloro-2-nitrophenyl)methanone (16). Prepared according to Procedure B using 1-(5-chloro-2-methylphenyl)piperazine (61.0 mg, 0.29 mmol), 4-chloro-2-nitrobenzoic acid (93.0 mg, 0.46 mmol), DMAP (8.0 mg, 0.07 mmol), and EDC·HCl (143.0 mg, 0.75 mmol) in DMF (1 mL). Yield 62 mg (54%) as a colorless thick oil. ^1H NMR (400 MHz, $CDCl_3$) δ 8.21 (d, J = 2.1 Hz, 1H), 7.72 (dd, J = 8.1, 2.1 Hz, 1H), 7.41 (d, J = 8.1 Hz, 1H), 7.12 (d, J = 8.0 Hz, 1H), 7.05−6.91 (m, 2H), 3.97 (s, 2H), 3.38 (t, J = 5.0 Hz, 2H), 3.14−2.75 (m, 4H), 2.28 (s, 3H); ^{13}C NMR (101 MHz, $CDCl_3$) δ 165.62, 151.7, 146.0, 135.9, 134.6, 132.1, 131.9, 131.1, 131.05, 129.3, 125.1, 123.85, 119.9, 51.3, 51.2, 47.3, 42.4, 17.4; HRMS calculated for $C_{18}H_{17}Cl_2N_3O_3$ $[M + H]^+$ 394.0722, found 394.0720.

(4-(5-Chloro-2-methylphenyl)piperazin-1-yl)(2-chloro-3-nitrophenyl)methanone (17). Prepared according to Procedure B using 1-(5-chloro-2-methylphenyl)piperazine (53.0 mg, 0.25 mmol), 2-chloro-3-nitrobenzoic acid (102.0 mg, 0.50 mmol), DMAP (3.0 mg, 0.03 mmol), and EDC·HCl (114.0 mg, 0.59 mmol) in DMF (1.5 mL). Yield 45 mg (45%) as a colorless thick oil. ^1H NMR (400 MHz, $CDCl_3$) δ 7.79 (dd, J = 7.6, 2.1 Hz, 1H), 7.51−7.40 (m, 2H), 7.03 (d, J = 8.1 Hz, 1H), 6.91 (dd, J = 8.1, 2.1 Hz, 1H), 6.87 (d, J = 2.1 Hz, 1H), 4.00−3.81 (m, 2H), 3.44−3.21 (m, 2H), 3.00−2.68 (m, 4H), 2.19 (s, 3H); ^{13}C NMR (101 MHz, $CDCl_3$) δ 164.9, 151.6, 148.7, 138.8, 132.2, 131.9, 131.1, 131.0, 128.2, 125.7, 123.9, 123.3, 119.8, 51.8, 51.5, 47.2, 42.3, 17.4; HRMS calculated for $C_{18}H_{17}Cl_2N_3O_3$ $[M + Na]^+$ 416.0539, found 416.0513.

(4-(5-Chloro-2-methylphenyl)piperazin-1-yl)(3-chloro-5-nitrophenyl)methanone (18). Prepared according to Procedure B using 1-(5-chloro-2-methylphenyl)piperazine (57.0 mg, 0.27 mmol), 3-chloro-5-nitrobenzoic acid (103.0 mg, 0.51 mmol), DMAP (3.0 mg, 0.03 mmol), and EDC·HCl (115.0 mg, 0.60 mmol) in DMF (1.5 mL). Yield 92 mg (86%) as a colorless thick oil. ^1H NMR (400 MHz, $CDCl_3$) δ 8.19 (t, J = 2.0 Hz, 1H), 8.10 (dd, J = 2.1, 1.4 Hz, 1H), 7.69 (t, J = 1.7 Hz, 1H), 7.03 (d, J = 8.0 Hz, 1H), 6.95−6.84 (m, 2H), 3.85 (s, 2H), 3.49 (s, 2H), 2.85 (d, J = 27.0 Hz, 4H), 2.19 (s, 3H); ^{13}C NMR (101 MHz, $CDCl_3$) δ 166.4, 151.5, 148.6, 138.6, 136.1, 133.2, 132.2, 131.9, 131.0, 124.85, 124.0, 120.4, 119.9, 51.8, 51.5, 48.2, 42.9, 17.4; HRMS calculated for $C_{18}H_{17}Cl_2N_3O_3$ $[M + H]^+$ 394.0722, found 394.0671.

(4-(5-Chloro-2-methylphenyl)piperazin-1-yl)(3-chloro-4-nitrophenyl)methanone (19). Prepared according to Procedure B using 1-(5-chloro-2-methylphenyl)piperazine (58.0 mg, 0.27 mmol), 3-chloro-4-nitrobenzoic acid (103.0 mg, 0.51 mmol), DMAP (3.0 mg, 0.03 mmol), and EDC·HCl (115.0 mg, 0.60 mmol) in DMF (1.5 mL). Yield 96 mg (90%) as a colorless thick oil. ^1H NMR (400 MHz, $CDCl_3$) δ 7.92 (d, J = 8.2 Hz, 1H), 7.62 (d, J = 1.7 Hz, 1H), 7.46 (dd, J = 8.3, 1.7 Hz, 1H), 7.10 (d, J = 8.1 Hz, 1H), 6.98 (dd, J = 8.0, 2.1 Hz, 1H), 6.94 (s, 1H), 3.91 (s, 2H), 3.53 (s, 2H), 2.91 (d, J = 40.9 Hz, 4H), 2.26 (s, 3H); ^{13}C NMR (101 MHz, $CDCl_3$) δ 166.7, 151.5, 148.2, 140.7, 132.2, 131.85, 131.0, 130.55, 127.7, 126.2, 125.95, 123.9, 119.8, 51.9, 51.45, 48.1, 42.7, 17.4; HRMS calculated for $C_{18}H_{17}Cl_2N_3O_3$ $[M + H]^+$ 394.0720, found 394.0701.

(4-(5-Chloro-2-methylphenyl)piperazin-1-yl)(4-fluoro-3-nitrophenyl)methanone (20). Prepared according to Procedure B using 1-(5-chloro-2-methylphenyl)piperazine (52.0 mg, 0.25 mmol), 4-fluoro-3-nitrobenzoic acid (75.0 mg, 0.40 mmol), DMAP (3.0 mg, 0.025 mmol), and EDC·HCl (100.0 mg, 0.52 mmol) in DMF (1.5 mL). Yield 77 mg (83%) as a colorless thick oil. ^1H NMR (400 MHz, $CDCl_3$) δ 8.19 (dd, J = 7.0, 2.2 Hz, 1H), 7.78 (ddd, J = 8.6, 4.2, 2.2 Hz, 1H), 7.40 (dd, J = 10.4, 8.5 Hz, 1H), 7.12 (d, J = 8.1 Hz, 1H), 7.05−6.91 (m, 2H), 3.77 (m, 6 Hz, 4H), 3.12−2.73 (m, 4H), 2.29 (s, 3H); ^{13}C NMR (101 MHz, $CDCl_3$, including ^{19}F-coupling peaks) δ 166.9, 157.4, 154.7, 151.6, 137.2, 137.1, 134.6, 134.5, 132.6, 132.5, 132.2, 132.1, 131.9, 131.05, 125.4, 125.4, 123.9, 119.9, 119.8, 119.1, 118.9, 51.7, 51.6, 51.4, 48.3, 43.0, 17.4; HRMS calculated for $C_{18}H_{17}ClFN_3O_3$ $[M + H]^+$ 378.1015, found 378.0985.

(4-Bromo-3-nitrophenyl)(4-(5-chloro-2-methylphenyl)-piperazin-1-yl)methanone (21). Prepared according to Procedure B using 1-(5-chloro-2-methylphenyl)piperazine (59.0 mg, 0.28 mmol), 4-bromo-3-nitrobenzoic acid (105.0 mg, 0.43 mmol),

https://dx.doi.org/10.1021/acs.jmedchem.0c01482
J. Med. Chem. 2020, 63, 14054−14066

DMAP (3.0 mg, 0.03 mmol), and EDC·HCl (100.0 mg, 0.52 mmol) in DMF (1.5 mL). Yield 115 mg (93%) as a colorless thick oil. ^{1}H NMR (400 MHz, $CDCl_3$) δ 7.94 (d, J = 2.0 Hz, 1H), 7.82 (d, J = 8.2 Hz, 1H), 7.53 (dd, J = 8.2, 2.0 Hz, 1H), 7.12 (d, J = 8.1 Hz, 1H), 7.04−6.92 (m, 2H), 4.04−3.46 (m, 4H), 2.92 (bs, 4H), 2.28 (s, 3H); ^{13}C NMR (101 MHz, $CDCl_3$) δ 166.9, 151.6, 149.7, 136.1, 135.5, 132.2, 131.9, 131.75, 131.05, 124.5, 123.9, 119.9, 116.0, 51.7, 48.2, 42.9, 17.4; HRMS calculated for $C_{18}H_{17}BrClN_3O_3$ $[M + H]^+$ 438.0215, found 438.0190.

(4-(5-Chloro-2-methylphenyl)piperazin-1-yl)(4-iodo-3-nitrophenyl)methanone (22). Prepared according to Procedure B using 1-(5-chloro-2-methylphenyl)piperazine (55.0 mg, 0.26 mmol), 4-iodo-3-nitrobenzoic acid (143.0 mg, 0.49 mmol), DMAP (3.0 mg, 0.03 mmol), and EDC·HCl (100.0 mg, 0.52 mmol) in DMF (1.5 mL). Yield 115 mg (91%) as a colorless thick oil. ^{1}H NMR (400 MHz, $CDCl_3$) δ 8.03 (d, J = 8.1 Hz, 1H), 7.85 (d, J = 1.9 Hz, 1H), 7.27 (dd, J = 8.1, 2.0 Hz, 1H), 7.02 (d, J = 8.0 Hz, 1H), 6.96−6.84 (m, 2H), 4.02−3.18 (m, 3H), 2.85 (m, 5H), 2.19 (s, 3H); ^{13}C NMR (101 MHz, $CDCl_3$) δ 167.0, 152.9, 151.6, 142.4, 136.9, 132.2, 131.9, 131.8, 131.05, 124.2, 123.9, 119.9, 88.0, 51.7, 48.2, 42.8, 17.4; HRMS calculated for $C_{18}H_{17}ClIN_3O_3$ $[M + H]^+$ 486.0084, found 486.0076.

(4-(5-Chloro-2-methylphenyl)piperazin-1-yl)(3-nitro-4-(trifluoromethoxy)phenyl)methan-one (23). Prepared according to Procedure B using 1-(5-chloro-2-methylphenyl)piperazine (51.0 mg, 0.24 mmol), 3-nitro-4-(trifluoromethoxy)benzoic acid (51.0 mg, 0.20 mmol), DMAP (4.0 mg, 0.03 mmol), and EDC·HCl (47.0 mg, 0.24 mmol) in DMF (1 mL). Yield 54 mg (60%) as a colorless thick oil. ^{1}H NMR (400 MHz, $CDCl_3$) δ 8.00 (d, J = 2.1 Hz, 1H), 7.69 (dd, J = 8.5, 2.1 Hz, 1H), 7.46 (dq, J = 8.6, 1.5 Hz, 1H), 7.04 (d, J = 8.0 Hz, 1H), 6.97−6.86 (m, 2H), 4.00−3.38 (m, 4H), 2.84 (m, 4H), 2.20 (s, 3H); ^{13}C NMR (101 MHz, $CDCl_3$) δ 166.5, 151.5, 142.4, 142.0, 142.0, 135.3, 133.0, 132.2, 131.9, 131.0, 125.05, 124.0, 123.38, 123.37, 121.4, 119.9, 118.8, 51.55, 48.3, 47.25, 42.9, 17.42, 17.36; HRMS calculated for $C_{19}H_{17}ClF_3N_3O_4$ $[M + H]^+$ 444.0932, found 444.0920.

(4-Chloro-3-nitrophenyl)(4-(3-(prop-2-yn-1-yloxy)phenyl)-piperazin-1-yl)methanone (24). Intermediate (4-chloro-3-nitrophenyl)(4-(3-hydroxyphenyl)piperazin-1-yl)methanone was prepared according to Procedure A using 4-chloro-3-nitrobenzoyl chloride (1.05 g, 4.75 mmol), 1-(3-hydroxyphenyl)piperazine (1.30 g, 7.29 mmol), and Et_3N (4 mL, 28.69 mmol) in THF (20 mL). The reaction mixture was diluted with EtOAc (50 mL) and washed with H_2O (3 × 50 mL) and brine (50 mL). The collected organics were dried (Na_2SO_4) and concentrated under reduced pressure to give (4-chloro-3-nitrophenyl)(4-(3-hydroxyphenyl)piperazin-1-yl)methanone as a light-yellow solid. Without further purification, (4-chloro-3-nitrophenyl)(4-(3-hydroxyphenyl)piperazin-1-yl)methanone (180.0 mg, 0.49 mmol) was dissolved in DMF (5 mL). After addition of K_2CO_3 (500.0 mg, 3.62 mmol) and propargyl bromide (80% in PhMe, 0.25 mL, 2.24 mmol), the resulting mixture was stirred at room temperature for 16 h. The reaction mixture was diluted with CH_2Cl_2 (20 mL) and quenched with H_2O (20 mL). The organic layer was washed with H_2O (3 × 20 mL) and brine (20 mL), dried (Na_2SO_4), and concentrated under reduced pressure. The residue was purified by flash chromatography (gradient of 0−50% EtOAc in hexane) to yield 97 mg (49%) of **24** as a brown gummy solid. ^{1}H NMR (400 MHz, $CDCl_3$) δ 7.96 (d, J = 1.8 Hz, 1H), 7.71−7.47 (m, 2H), 7.19 (ddd, J = 8.4, 7.2, 1.5 Hz, 1H), 6.64−6.28 (m, 3H), 4.66 (d, J = 2.4 Hz, 2H), 3.73 (m, 4H), 3.19 (m, 4H), 2.52 (t, J = 2.4 Hz, 1H); ^{13}C NMR (101 MHz, $CDCl_3$) δ 166.7, 158.6, 152.0, 147.8, 135.3, 132.3, 131.85, 130.0, 128.6, 124.7, 110.2, 106.25, 104.2, 78.6, 75.6, 55.8, 49.6, 47.6, 42.35; HRMS calculated for $C_{20}H_{18}ClN_3O_4$ $[M + H]^+$ 400.1059, found 400.1056.

(4-Methyl-3-nitrophenyl)(4-(3-(prop-2-yn-1-yloxy)phenyl)-piperazin-1-yl)methanone (25). Intermediate (4-(3-hydroxyphenyl)piperazin-1-yl)(4-methyl-3-nitrophenyl)methanone was prepared according to Procedure B using 4-methyl-3-nitrobenzoic acid (500.0 mg, 2.76 mmol), 1-(3-hydroxyphenyl)piperazine (740.0 mg, 4.14 mmol), DMAP (34.0 mg, 0.27 mmol), and EDC·HCl (800.0 mg, 4.14 mmol) in DMF (5 mL). The reaction mixture was diluted with EtOAc (40 mL) and washed with H_2O (3 × 40 mL) and brine (40 mL). The organic phase was dried (Na_2SO_4) and concentrated under reduced pressure to yield crude (4-(3-hydroxyphenyl)-piperazin-1-yl)(4-methyl-3-nitrophenyl)methanone as a light-yellow solid. Without further purification, crude (4-(3-hydroxyphenyl)-piperazin-1-yl)(4-methyl-3-nitrophenyl)methanone (71.0 mg, 0.50 mmol) was dissolved in DMF (1.5 mL). After addition of K_2CO_3 (207.0 mg, 1.50 mmol) and propargyl bromide (80% in PhMe, 150 □L, 1.20 mmol), the mixture was stirred at room temperature for 16 h. The reaction mixture was diluted with CH_2Cl_2 (20 mL) and quenched with H_2O (20 mL). The organic layer was washed with H_2O (3 × 20 mL) and brine (20 mL), dried (Na_2SO_4), and concentrated under reduced pressure. The residue was purified by flash chromatography (gradient of 0−50% EtOAc in hexane) to yield 35 mg (71%) of **25** as a colorless thick oil. ^{1}H NMR (400 MHz, $CDCl_3$) δ 7.98 (d, J = 1.7 Hz, 1H), 7.52 (dd, J = 7.8, 1.7 Hz, 1H), 7.36 (d, J = 7.8 Hz, 1H), 7.13 (t, J = 8.5 Hz, 1H), 6.55−6.41 (m, 3H), 4.60 (d, J = 2.4 Hz, 2H), 3.68 (m, 4H), 3.14 (bs, 4H), 2.57 (s, 3H), 2.45 (t, J = 2.4 Hz, 1H); ^{13}C NMR (101 MHz, $CDCl_3$) δ 167.8, 158.65, 152.1, 149.0, 135.4, 134.55, 133.25, 131.6, 130.0, 123.7, 110.2, 106.25, 104.2, 78.6, 75.5, 55.8, 49.5, 47.6, 42.3, 20.4; HRMS calculated for $C_{21}H_{21}N_3O_4$ $[M + H]^+$ 380.1605, found 380.1604.

4-(4-(3,5-Dimethoxyphenyl)piperazine-1-carbonyl)-2-nitro-benzaldehyde (26). Prepared according to Procedure B using 1-(3,5-dimethoxyphenyl)piperazine (130.0 mg, 0.58 mmol), 4-formyl-3-nitrobenzoic acid (125.0 mg), DMAP (6.0 mg, 0.05 mmol), and EDC·HCl (200.0 mg, 1.04 mmol) in DMF (1 mL). Yield 57 mg as a colorless thick oil. ^{1}H NMR (400 MHz, $CDCl_3$) δ 10.35 (s, 1H), 8.10 (d, J = 1.5 Hz, 1H), 7.93 (d, J = 7.8 Hz, 1H), 7.75 (dd, J = 7.8, 1.5 Hz, 1H), 6.00 (s, 3H), 4.01−3.76 (m, 2H), 3.70 (s, 6H), 3.49 (d, J = 19.3 Hz, 2H), 3.14 (d, J = 53.0 Hz, 4H); ^{13}C NMR (101 MHz, $CDCl_3$) δ 187.3, 166.5, 161.6, 152.55, 149.5, 141.0, 132.4, 131.9, 130.2, 123.5, 95.88, 92.6, 55.3, 49.8, 49.4, 47.5, 42.3; HRMS calculated for $C_{20}H_{21}N_3O_6$ $[M + H]^+$ 400.1503, found 400.1501.

Cytotoxicity Assay. Mouse SCLC cell lines were seeded in duplicate in 96-well plates, 10,000 cells and 200 μL of DMEM media (5% FBS) per well. After overnight incubation, compounds were dispensed using a D300e Digital Dispenser (TECAN) in 10-point dose response manner using $^1/_2$ log dilutions. Cell viability was assessed after 72 h using CellTiter-Glo luminescent cell viability assay (Promega, #G7571). The CellTiter-Glo reagent was diluted by adding PBS/Triton-X (1%) (1:1 ratio). Each value was normalized to cells treated with DMSO, and the IC_{50} values were calculated using GraphPad Prism software.

Cross-Linking Experiments. Murine SCLC cells, 518T2, were plated in 12-well plates (1 million cells per well) in 1 mL of DMEM media (5% FBS) per well. The following day, probe **24** or probe **25** dissolved in DMSO was dispensed at increasing concentrations (50 nM to 50 μM). After 1.5 h incubation at 37 °C in 5% CO_2, cells were washed gently with PBS and lysed in 1% SDS Buffer A (50 mM HEPES, pH 7.4, 10 mM KCl, 2 mM $MgCl_2$), freshly supplemented with 1:10,000 benzonase (Sigma-Aldrich). For competition experiments, analogs dissolved in DMSO were dispensed at increasing concentrations (100 nM to 50 μM) first and murine SCLC cells, 518T2, were plated in 12-well plates (1 million cells per well) in 1 mL DMEM media (5% FBS) per well. The following day, either probe **24** or probe **25** was dispensed in DMSO at increasing concentrations (50 nM to 50 μM). After 1.5 h incubation at 37 °C in 5% CO_2, cells were washed gently with PBS and lysed in 1% SDS Buffer A (50 mM HEPES, pH 7.4, 10 mM KCl, 2 mM $MgCl_2$), freshly supplemented with 1:10,000 benzonase (Sigma-Aldrich). Click chemistry was performed as previously described.[29]

Protein Purification. For purification experiments, cells were plated in 15 cm dishes at a large scale to obtain 100 mg of protein per condition and allowed to adhere overnight. The following day, cells were subjected to photocross-linking experiments described above. Instead of 25 μM Alexa Fluor 532 azide, 100 μM diazo biotin azide (Click Chemistry Tools, #1041) was used for the click reaction. Proteins were precipitated with four volumes of acetone cooled to −80 °C, and the insoluble protein pellets were centrifuged at 6000g and then resolubilized in PBS (4% SDS) overnight. The insoluble

https://dx.doi.org/10.1021/acs.jmedchem.0c01482
J. Med. Chem. 2020, 63, 14054−14066

material was pelleted by centrifugation at 20,000*g*, and the soluble supernatant was filtered using 0.45 μm and 0.22 μm filters. Streptavidin agarose beads (Solu-link) were added and incubated with the resolubilized protein for 1 h at 25 °C. Beads were washed three times with 4% SDS in PBS, and the protein was eluted at 95 °C in Laemmli sample buffer. Proteins were resolved by SDS-PAGE, and the gel was stained with silver stain (Pierce, #24612). For proteomics analysis, samples were run until proteins enter into the SDS-PAGE gel, and each sample was cut and sent for shotgun analysis using LC–MS/MS.

Proteomics Analysis. Gel band samples were digested overnight with trypsin (Pierce) following reduction and alkylation with DTT and iodoacetamide (Sigma-Aldrich). The samples then underwent solid-phase extraction cleanup with an Oasis HLB plate (Waters), and the resulting samples were injected onto an Orbitrap Fusion Lumos mass spectrometer coupled to an Ultimate 3000 RSLC-Nano liquid chromatography system. Samples were injected onto a 75 μm i.d., 75 cm-long EasySpray column (Thermo) and eluted with a gradient from 0 to 28% buffer B over 90 min. Buffer A contained 2% (v/v) ACN and 0.1% formic acid in water, and buffer B contained 80% (v/v) ACN, 10% (v/v) trifluoroethanol, and 0.1% formic acid in water. The mass spectrometer was operated in positive ion mode with a source voltage of 1.5 kV and an ion transfer tube temperature of 275 °C. MS scans were acquired at 120,000 resolution in the Orbitrap, and up to 10 MS/MS spectra were obtained in the ion trap for each full spectrum acquired using higher-energy collisional dissociation (HCD) for ions with charges 2–7. Dynamic exclusion was set for 25 s after an ion was selected for fragmentation.

Raw MS data files were analyzed using Proteome Discoverer v2.4 SP1 (Thermo), with peptide identification performed using Sequest HT searching against the human protein database from UniProt. Fragment and precursor tolerances of 10 ppm and 0.6 Da were specified, respectively, and three missed cleavages were allowed. Carbamidomethylation of Cys was set as a fixed modification, with oxidation of Met set as a variable modification. The false-discovery rate cutoff was 1% for all peptides.

Proteomic data for samples **24** and **25** are accessible at MassIVE accession number: MSV000085897 (ftp://massive.ucsd.edu/MSV000085897/).

Expression and Purification of β_3 Human $\alpha\beta$-Tubulin. Human $\alpha\beta$-tubulin (non-tagged TUBA1B gene and TUBB3 gene with a cleavable His-tag at the C-terminus) was expressed in insect cells as described previously.[23] Briefly, Tni cells (Expression Systems) and ESF-921 insect cell medium (Expression Systems) were used for expression. Cells were harvested approximately ∼42 h post-infection, re-suspended in 3 volumes of lysis buffer (25 mM Hepes, pH 7.4, 30 mM imidazole, 1 mM $MgSO_4$, 50 μM GTP), and lysed using a glass dounce. Lysate was clarified by centrifugation, and recombinant tubulin was purified by Ni-affinity (5 mL Ni-NTA column, TaKaRA) and anion exchange (4 mL Source-Q column, GE Amersham) chromatography. The His-tag was removed by TEV protease (2 h on ice using a TEV at 0.2 mg/mL final concentration) prior to anion exchange chromatography. Peak fractions were pooled, concentrated to 15–20 μM, buffer-exchanged to BRB80 with 50 μM GTP, flash-frozen on liquid nitrogen in 100 μL aliquots, and stored at −80 °C.

Microtubule Dynamics Assays. Microtubule dynamics were measured by time-lapse differential interference contrast microscopy, as described previously.[30−32] Temperature was maintained at 30 °C using an enclosure fit to the microscope body, and the microscope was controlled using a MicroManager.[33] Briefly, assays were performed in flow chambers using GMPCPP seeds made from brain tubulin (5% biotinylated; PurSolutions) attached to coverslips using neutravidin (Invitrogen). Microtubule dynamics were measured in the following buffer (144 mM PIPES, pH 6.9, 3.6 mM MgCl2, 50 mM KCl, 1 mM GTP, 0.1 mg/mL BSA, 0.07% methylcellulose, and 4% DMSO final concentration). DMSO was the solvent where compounds were dissolved in. We used a higher than typical concentration of PIPES because microtubule dynamics were not robustly observable at lower concentrations for the recombinant human tubulin. Images were acquired every 50 ms (using a Photometrics Prime95B camera) and averaged in batches of 30 to improve signal to noise. Recordings typically lasted for 30 min. Microtubule growing rates were obtained from kymographs prepared using ImageJ.[33]

■ ASSOCIATED CONTENT

Supporting Information

The Supporting Information is available free of charge at https://pubs.acs.org/doi/10.1021/acs.jmedchem.0c01482.

List of proteins by mass spectrometry analysis in tubulin-probe purification with analog **24** compared to compound **25** (XLSX)

Somatic mutations identified in resistant clones to compound **27** compared to parental 319N1-M2KO cells (XLSX)

Supplementary tables (benzamide analogs and proteins enriched), supplementary figures (dose–response curves, SDS-PAGE full gel images, and kymographs), methods (Selection of Resistant Clones; *Tubb5*^{T238A} Point Mutation; Whole Exome Sequence Analysis; and Identification of Recurrently Mutated Genes in Sulfonamide **27**-Resistant Clones), and copies of ^{1}H and ^{13}C spectra, HPLC chromatograms and HRMS data (PDF)

Molecular formula strings (CSV)

■ AUTHOR INFORMATION

Corresponding Authors

Jef K. De Brabander − *Department of Biochemistry and Harold C. Simmons Comprehensive Cancer Center, University of Texas Southwestern Medical Center, Dallas, Texas 75390, United States;* orcid.org/0000-0001-8816-5798; Email: jef.debrabander@utsouthwestern.edu

David G. McFadden − *Department of Internal Medicine, Division of Endocrinology, Department of Biochemistry, Harold C. Simmons Comprehensive Cancer Center, and Program in Molecular Medicine, University of Texas Southwestern Medical Center, Dallas, Texas 75390, United States;* orcid.org/0000-0001-8466-2199; Email: david.mcfadden@utsouthwestern.edu

Authors

Juan Manuel Povedano − *Department of Internal Medicine, Division of Endocrinology and Department of Biochemistry, University of Texas Southwestern Medical Center, Dallas, Texas 75390, United States;* orcid.org/0000-0002-8384-6540

Rameshu Rallabandi − *Department of Biochemistry, University of Texas Southwestern Medical Center, Dallas, Texas 75390, United States*

Xin Bai − *Department of Internal Medicine, Division of Endocrinology and Department of Biochemistry, University of Texas Southwestern Medical Center, Dallas, Texas 75390, United States*

Xuecheng Ye − *Department of Biophysics, University of Texas Southwestern Medical Center, Dallas, Texas 75390, United States*

Joel Liou − *Department of Internal Medicine, Division of Endocrinology and Department of Biochemistry, University of Texas Southwestern Medical Center, Dallas, Texas 75390, United States*

Hong Chen − *Department of Biochemistry and Harold C. Simmons Comprehensive Cancer Center, University of Texas*

Southwestern Medical Center, Dallas, Texas 75390, United States

Jiwoong Kim − *Quantitative Biomedical Research Center, Department of Population and Data Sciences, University of Texas Southwestern Medical Center, Dallas, Texas 75390, United States*

Yang Xie − *Quantitative Biomedical Research Center, Department of Population and Data Sciences, University of Texas Southwestern Medical Center, Dallas, Texas 75390, United States*

Bruce Posner − *Department of Biochemistry and Harold C. Simmons Comprehensive Cancer Center, University of Texas Southwestern Medical Center, Dallas, Texas 75390, United States*

Luke Rice − *Department of Biophysics, University of Texas Southwestern Medical Center, Dallas, Texas 75390, United States*

Complete contact information is available at: https://pubs.acs.org/10.1021/acs.jmedchem.0c01482

Author Contributions

[▽]J.M.P. and R.R. contributed equally to this work

Author Contributions

All authors have given approval to the final version of the manuscript.

Notes

The authors declare no competing financial interest.

■ ACKNOWLEDGMENTS

This work was funded through a UT Southwestern Dean's Circle of Friends Pilot Synergy Grant. J.K.D.B. acknowledges support from the Welch Foundation (Grant I-1422) and holds the Julie and Louis Beecherl, Jr., Chair in Medical Science. D.G.M. acknowledges support from the Welch Foundation (Grant I-2040), the Disease Oriented Scholars Program at UT Southwestern, a Clinical Investigator Award from the Damon Runyon Cancer Research Foundation (102-19), the Cancer Prevention and Research Institute of Texas (RR140084 and RP190141), and the National Cancer Institute of the NIH (U54CA231649). J.M.P. is supported by a fellowship from the Chilton Family Foundation. HRMS data were obtained from the Shimadzu Center for Advanced Analytical Chemistry (SCAAC) at UT Arlington. Work in the laboratory of L.M.R. was supported by the NIH (R01-GM098543) and the Welch Foundation (Grant I-1908). Andrew Lemoff and colleagues at the UT Southwestern Medical Center Proteomics Core Facility performed mass spectrometry analysis on benzamide-bound proteins. We thank John Minna and Adi Gazdar for sharing human SCLC cell lines. We thank Deepak Nijhawan for critically reading the manuscript and for numerous helpful discussions. We thank Kuanqing Liu for critically reading the manuscript.

■ REFERENCES

(1) McFadden, D. G.; Papagiannakopoulos, T.; Taylor-Weiner, A.; Stewart, C.; Carter, S. L.; Cibulskis, K.; Bhutkar, A.; McKenna, A.; Dooley, A.; Vernon, A.; Sougnez, C.; Malstrom, S.; Heimann, M.; Park, J.; Chen, F.; Farago, A. F.; Dayton, T.; Shefler, E.; Gabriel, S.; Getz, G.; Jacks, T. Genetic and clonal dissection of murine small cell lung carcinoma progression by genome sequencing. *Cell* **2014**, *156*, 1298−1311.

(2) Calbo, J.; Meuwissen, R.; van Montfort, E.; van Tellingen, O.; Berns, A. Genotype-phenotype relationships in a mouse model for human small-cell lung cancer. *Cold Spring Harbor Symp. Quant. Biol.* **2005**, *70*, 225−232.

(3) Gazdar, A. F.; Savage, T. K.; Johnson, J. E.; Berns, A.; Sage, J.; Linnoila, R. I.; MacPherson, D.; McFadden, D. G.; Farago, A.; Jacks, T.; Travis, W. D.; Brambilla, E. The comparative pathology of genetically engineered mouse models for neuroendocrine carcinomas of the lung. *J Thorac Oncol* **2015**, *10*, 553−564.

(4) Meuwissen, R.; Linn, S. C.; Linnoila, R. I.; Zevenhoven, J.; Mooi, W. J.; Berns, A. Induction of small cell lung cancer by somatic inactivation of both Trp53 and Rb1 in a conditional mouse model. *Cancer Cell* **2003**, *4*, 181−189.

(5) Nile, A. H.; Tripathi, A.; Yuan, P.; Mousley, C. J.; Suresh, S.; Wallace, I. M.; Shah, S. D.; Pohlhaus, D. T.; Temple, B.; Nislow, C.; Giaever, G.; Tropsha, A.; Davis, R. W.; St Onge, R. P.; Bankaitis, V. A. PITPs as targets for selectively interfering with phosphoinositide signaling in cells. *Nat. Chem. Biol.* **2014**, *10*, 76−84.

(6) The trifluoromethoxy group has been described as a leaving group in S_NAr, see: Marrec, O.; Billard, T.; Vors, J.-P.; Pazenok, S.; Langlois, B. R. A New and direct trifluoromethoxylation of aliphatic substrates with 2,4-dinitro(trifluoromethoxy)benzene. *Adv. Synth. Catal.* **2010**, *352*, 2831−2837.

(7) Theodoropoulos, P. C.; Wang, W.; Budhipramono, A.; Thompson, B. M.; Madhusudhan, N.; Mitsche, M. A.; McDonald, J. G.; De Brabander, J. K.; Nijhawan, D. A medicinal chemistry-driven approach identified the sterol isomerase EBP as the molecular target of TASIN colorectal cancer toxins. *J. Am. Chem. Soc.* **2020**, *142*, 6128−6138.

(8) Speers, A. E.; Cravatt, B. F. Profiling enzyme activities in vivo using click chemistry methods. *Chem. Biol.* **2004**, *11*, 535−546.

(9) Wright, A. T.; Cravatt, B. F. Chemical proteomic probes for profiling cytochrome p450 activities and drug interactions in vivo. *Chem. Biol.* **2007**, *14*, 1043−1051.

(10) Lee, G.; Elwood, F.; McNally, J.; Weiszmann, J.; Lindstrom, M.; Amaral, K.; Nakamura, M.; Miao, S.; Cao, P.; Learned, R. M.; Chen, J. L.; Li, Y. T0070907, a selective ligand for peroxisome proliferator-activated receptor gamma, functions as an antagonist of biochemical and cellular activities. *J Biol Chem* **2002**, *277*, 19649−19657.

(11) Harris, G.; Schaefer, K. L. The microtubule-targeting agent T0070907 induces proteasomal degradation of tubulin. *Biochem. Biophys. Res. Commun.* **2009**, *388*, 345−349.

(12) Schaefer, K. L.; Takahashi, H.; Morales, V. M.; Harris, G.; Barton, S.; Osawa, E.; Nakajima, A.; Saubermann, L. J. PPARgamma inhibitors reduce tubulin protein levels by a PPARgamma, PPARdelta and proteasome-independent mechanism, resulting in cell cycle arrest, apoptosis and reduced metastasis of colorectal carcinoma cells. *Int. J. Cancer* **2007**, *120*, 702−713.

(13) Yang, J.; Li, Y.; Yan, W.; Li, W.; Qiu, Q.; Ye, H.; Chen, L. Covalent modification of Cys-239 in β-tubulin by small molecules as a strategy to promote tubulin heterodimer degradation. *J Biol Chem* **2019**, *294*, 8161−8170.

(14) Frankmoelle, W. P.; Medina, J. C.; Shan, B.; Narbut, M. R.; Beckmann, H. Glutathione S-transferase metabolism of the antineoplastic pentafluorophenylsulfonamide in tissue culture and mice. *Drug Metab. Dispos.* **2000**, *28*, 951−958.

(15) Shan, B.; Medina, J. C.; Santha, E.; Frankmoelle, W. P.; Chou, T.-C.; Learned, R. M.; Narbut, M. R.; Stott, D.; Wu, P.; Jaen, J. C.; Rosen, T.; Timmermans, P. B. M. W. M.; Beckmann, H. Selective, covalent modification of β-tubulin residue Cys-239 by T138067, an antitumor agent with in vivo efficacy against multidrug-resistant tumors. *Proc. Natl. Acad. Sci. U. S. A.* **1999**, *96*, 5686−5691.

(16) Bai, R.; Covell, D. G.; Pei, X.-F.; Ewell, J. B.; Nguyen, N. Y.; Brossi, A.; Hamel, E. Mapping the binding site of colchicinoids on β-tubulin. 2-Chloroacetyl-2-demethylthiocolchicine covalently reacts predominantly with cysteine 239 and secondarily with cysteine 354. *J Biol Chem* **2000**, *275*, 40443−40452.

(17) Steinmetz, M. O.; Prota, A. E. Microtubule-targeting agents: strategies to hijack the cytoskeleton. *Trends Cell Biol* **2018**, *28*, 776−792.

(18) Brouhard, G. J.; Rice, L. M. Microtubule dynamics: an interplay of biochemistry and mechanics. *Nat Rev Mol Cell Biol* **2018**, *19*, 451−463.
(19) Dumontet, C.; Jordan, M. A. Microtubule-binding agents: a dynamic field of cancer therapeutics. *Nat Rev Drug Discov* **2010**, *9*, 790−803.
(20) Ferlini, C.; Raspaglio, G.; Mozzetti, S.; Cicchillitti, L.; Filippetti, F.; Gallo, D.; Fattorusso, C.; Campiani, G.; Scambia, G. The seco-taxane IDN5390 is able to target class III β-tubulin and to overcome paclitaxel resistance. *Cancer Res.* **2005**, *65*, 2397−2405.
(21) Mozzetti, S.; Ferlini, C.; Concolino, P.; Filippetti, F.; Raspaglio, G.; Prislei, S.; Gallo, D.; Martinelli, E.; Ranelletti, F. O.; Ferrandina, G.; Scambia, G. Class III β-tubulin overexpression is a prominent mechanism of paclitaxel resistance in ovarian cancer patients. *Clin Cancer Res* **2005**, *11*, 298−305.
(22) Arnst, K. E.; Banerjee, S.; Chen, H.; Deng, S.; Hwang, D. J.; Li, W.; Miller, D. D. Current advances of tubulin inhibitors as dual acting small molecules for cancer therapy. *Med. Res. Rev.* **2019**, *39*, 1398−1426.
(23) Ye, X.; Kim, T.; Geyer, E. A.; Rice, L. M. Insights into allosteric control of microtubule dynamics from a buried β-tubulin mutation that causes faster growth and slower shrinkage. *Protein Sci.* **2020**, *29*, 1429−1439.
(24) Jost, M.; Chen, Y.; Gilbert, L. A.; Horlbeck, M. A.; Krenning, L.; Menchon, G.; Rai, A.; Cho, M. Y.; Stern, J. J.; Prota, A. E.; Kampmann, M.; Akhmanova, A.; Steinmetz, M. O.; Tanenbaum, M. E.; Weissman, J. S. Combined CRISPRi/a-based chemical genetic screens reveal that rigosertib is a microtubule-destabilizing agent. *Mol. Cell* **2017**, *68*, 210−223.e6 e6.
(25) Yang, J.; Yan, W.; Li, Y.; Niu, L.; Ye, H.; Chen, L. The natural compound withaferin A covalently binds to Cys239 of β-tubulin to promote tubulin degradation. *Mol. Pharmacol.* **2019**, *96*, 711−719.
(26) Povedano, J. M.; Liou, J.; Wei, D.; Srivatsav, A.; Kim, J.; Xie, Y.; McFadden, D. G. Engineering forward genetics into cultured cancer cells for chemical target identification. *Cell Chem. Biol.* **2019**, 1315−1321.e3.
(27) Machin, N. A.; Lee, J. M.; Barnes, G. Microtubule stability in budding yeast: characterization and dosage suppression of a benomyl-dependent tubulin mutant. *Mol. Biol. Cell* **1995**, *6*, 1241−1259.
(28) Thomas, J. H.; Neff, N. F.; Botstein, D. Isolation and characterization of mutations in the β-tubulin gene of Saccharomyces cerevisiae. *Genetics* **1985**, *111*, 715−734.
(29) Madhusudhan, N.; Hu, B.; Mishra, P.; Calva-Moreno, J. F.; Patel, K.; Boriack, R.; Ready, J. M.; Nijhawan, D. Target discovery of selective non-small-cell lung cancer toxins reveals inhibitors of mitochondrial complex I. *ACS Chem. Biol.* **2020**, *15*, 158−170.
(30) Geyer, E. A.; Burns, A.; Lalonde, B. A.; Ye, X.; Piedra, F. A.; Huffaker, T. C.; Rice, L. M. A mutation uncouples the tubulin conformational and GTPase cycles, revealing allosteric control of microtubule dynamics. *Elife* **2015**, *4*, No. e10113.
(31) Kim, T.; Rice, L. M. Long-range, through-lattice coupling improves predictions of microtubule catastrophe. *Mol. Biol. Cell* **2019**, *30*, 1451−1462.
(32) Majumdar, S.; Kim, T.; Chen, Z.; Munyoki, S.; Tso, S. C.; Brautigam, C. A.; Rice, L. M. An isolated CLASP TOG domain suppresses microtubule catastrophe and promotes rescue. *Mol. Biol. Cell* **2018**, *29*, 1359−1375.
(33) Edelstein, A.; Amodaj, N.; Hoover, K.; Vale, R.; Stuurman, N. Computer control of microscopes using μManager. *Curr Protoc Mol Biol* **2010**, *92*, 14.20.1−14.20.17.

https://dx.doi.org/10.1021/acs.jmedchem.0c01482
J. Med. Chem. 2020, 63, 14054−14066